Geological Magazine

www.cambridge.org/geo

Role of fluids on deformation in mid-crustal shear zones, Raft River Mountains, Utah

Raphaël Gottardi and Brendan Hughes

School of Geosciences, University of Louisiana at Lafayette, 611 McKinley Street, Lafayette, LA 70504, USA

Original Article

Cite this article: Gottardi R and Hughes B (2023) Role of fluids on deformation in mid-crustal shear zones, Raft River Mountains, Utah. *Geological Magazine* **159**: 2206–2218. https://doi.org/10.1017/S0016756822000231

Received: 14 December 2021
Revised: 9 March 2022
Accepted: 21 March 2022
First published online: 19 April 2022

Keywords:
metamorphic core complex; detachment shear zones; fluid flow; fluid–rock interaction; strain localization; brittle–ductile transition

Author for correspondence:
Raphaël Gottardi,
Email: gottardi@louisiana.edu

Abstract

Fluids are commonly invoked as the primary cause for weakening of detachment shear zones. However, fluid-related mechanisms such as pressure-solution, reaction-enhanced ductility, reaction softening and precipitation of phyllosilicates are not fully understood. Fluid-facilitated reaction and mass transport cause rheological weakening and strain localization, eventually leading to departure from failure laws derived in laboratory experiments. This study focuses on the Miocene Raft River detachment shear zone in northwestern Utah. The shear zone is localized in the Proterozoic Elba Quartzite, which unconformably overlies the Archaean basement, and consists of an alternating sequence of quartzite and muscovite-quartzite schist. In this study, we characterize fluid-related microstructures to constrain conditions that promoted brittle failure in a plastically deforming shear zone. Thin-section analyses reveal the presence of healed microcracks, transgranular fluid inclusion planes and grain boundary fluid inclusion clusters. Healed microcracks occur in three sets, one sub-perpendicular to the mylonitic foliation, and a set of two conjugate microcracks oriented at ~40–60° to the mylonitic foliation. Healed microfractures are filled with quartz, which has a distinct fabric, suggesting that microcracks healed while the shear zone was still at conditions favourable for quartz crystal plasticity. Transgranular fluid inclusion planes also occur in three sets, similar in orientation to the healed microfractures. Fluid inclusions commonly decorate grain and subgrain boundaries as inter- and intragranular clusters. Our results document ductile overprint of brittle microstructures, suggesting that, during exhumation, the Raft River detachment shear zone crossed the brittle–ductile transition repeatedly, providing pathways for fluids to permeate through this shear zone.

1. Introduction

Fluids play a critical role in controlling the chemical and physical behaviour of the crust and mantle (e.g. Caine *et al.* 1996; Hirschmann, 2006). Fluid–rock interaction controls rock deformation through a variety of processes including hydrolytic weakening (e.g. Griggs, 1967), pressure-solution creep (e.g. Shimizu, 1995) or metamorphic reactions (e.g. Ferry, 1994). Faults and shear zones are important structures that control fluid circulation from the upper to the lower crust (e.g. Reynolds & Lister, 1987; McCaig, 1988). Fluid circulation in the brittle upper crust is accommodated through faults and fractures that commonly increase porosity and permeability of the host rock, allowing fluids to penetrate to mid-crustal levels (e.g. McCaig, 1988; Sibson, 1992; Wehrens *et al.* 2016; Fig. 1). Faults also exhibit fault-valve behaviour, becoming highly permeable after seismic failure, channelling fluid discharge in the seismogenic zone (Sibson, 1990, 1992). This mechanism involves pre-seismic stress build-up causing increased dilatancy and drawing-in of fluid into the stressed rock, followed after seismic rupture by a pressure drop and fluid venting out of networks of microcracks (Reynolds & Lister, 1987; McCaig, 1988; Sibson, 1990). This fault-valve behaviour or 'seismic pumping' suggests that fluids may be one of the primary drivers of the seismic cycle (Cox, 2010; Miller, 2013; Zhu *et al.* 2020; Prando *et al.* 2020). In the ductile regime, fluid circulation is conceptually challenging (e.g. Connolly & Podladchikov, 2004). Recent studies have demonstrated that viscous flow can produce porosity in deforming rocks through dynamic recrystallization (Gilgannon *et al.* 2020) and creep cavitation processes (Fusseis *et al.* 2009; Menegon *et al.* 2015; Précigout *et al.* 2019; Dobe *et al.* 2021).

The brittle–ductile transition is therefore a critical zone to study fluid–rock interaction that occurs in faults and shear zones (e.g. Marchesini *et al.* 2019). Deformation at the brittle–ductile transition is cyclical, oscillating between brittle and ductile behaviour (e.g. Famin *et al.* 2004, 2005; Siebenaller *et al.* 2013, 2016; Carter *et al.* 2015; Compton *et al.* 2017). A switch in failure mode is typically attributed to a perturbation in one of the parameters controlling deformation, such as deviatoric stress, strain rate or pore fluid pressure. Detachment shear zones associated with metamorphic core complexes evolved at the brittle–ductile transition and are rapidly exhumed (e.g. review by Whitney *et al.* 2013 and references therein). These shear zones are

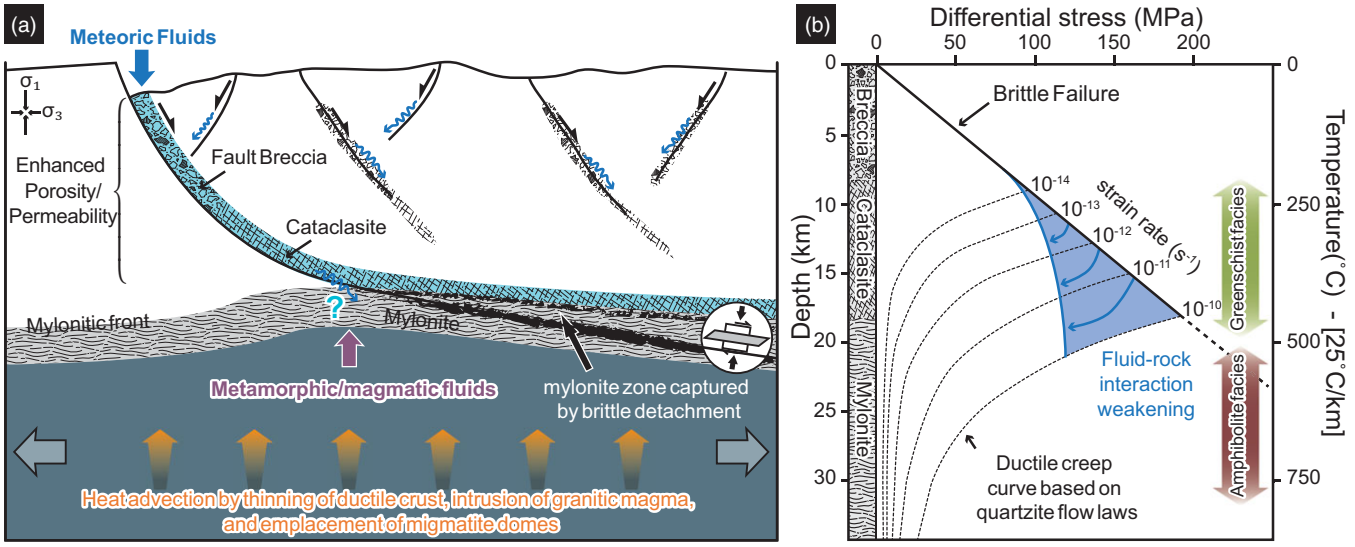

Fig. 1. (a) Fluid–rock interaction in a detachment system associated with the formation of a metamorphic core complex and (b) strength profile through the crust plotted with Coulomb frictional failure criterion for the upper crust and quartzite flow law for the lower crust, using a 25 °C/km geothermal gradient (modified from Gottardi *et al.* 2018).

therefore a prime candidate to study in detail fluid–rock interaction and brittle–ductile deformation.

Metamorphic core complexes form during orogenic collapse of an overthickened crust (e.g. review by Whitney *et al.* 2013 and references therein). Extension in the cool and brittle upper crust is accommodated by faulting and fracturing, providing pathways (high porosity/permeability fractures and faults) and head gradient (steep topography) for fluid infiltration (Fig. 1). The hot, ductile lower crust flows laterally. Because of this rheologic contrast between the upper and lower crust, combined with hydrolytic weakening, pressure-solution creep and metamorphic reactions in a fluid-saturated system, strain commonly localizes at the brittle–ductile transition, leading to the development of detachment shear zones. Progressive exhumation of the detachment shear zone leads to the formation of a metamorphic core complex.

In this contribution, we investigate the record of fluid–rock interaction at the brittle–ductile transition in the detachment shear zone associated with the Miocene Raft River metamorphic core complex (e.g. Wells *et al.* 2000). Previous work demonstrates abundant evidence of chemical, physical and isotopic water–rock interactions in this detachment shear zone (Gottardi *et al.* 2011, 2015; Methner *et al.* 2015). The goal of this study is to characterize fluid-related microstructures to constrain conditions that promoted brittle failure in a plastically deforming system.

2. Regional geology

2.a. The Raft River metamorphic core complex

The Raft River Mountains are located in northwestern Utah's portion of the Great Basin province and are a component of the larger Raft River–Albion–Grouse Creek metamorphic core complex (Fig. 2; Compton, 1975). The Raft River Mountains are composed of Archaean through Permian aged amphibolite- to greenschist-facies rocks. Following several episodes of contraction during the Mesozoic to early Cenozoic Sevier orogeny (Wells, 1997; Hoisch *et al.* 2002; Harris *et al.* 2007), the Raft River experienced two pulses of extension during Cenozoic time: an initial Eocene to early Oligocene (~42–37 Ma) extension along the W-rooted Middle Mountain shear zone (Saltzer & Hodges, 1988; Wells *et al.* 2000), and Oligo-Miocene extension (~25 to 15 Ma) along the top-to-the-E Raft River detachment shear zone (Wells *et al.* 2000; Wells, 2001; Gottardi *et al.* 2011; Gottardi & Teyssier, 2013).

The Raft River detachment fault and associated shear zone displace upper plate Neoproterozoic to Palaeozoic rocks ~30 km against Archaean to Proterozoic footwall rocks (Fig. 2; Wells *et al.* 2000). The footwall of the Raft River detachment shear zone is composed of the Green Creek Complex (Armstrong & Hills, 1967; Armstrong, 1968), which consists of ~2.55 Ga gneissic monzogranite that intrudes metatrondhjemite, metagabbro and hornblende-biotite schist (Armstrong, 1968; Compton *et al.* 1977; Miller, 1980; Todd, 1980) and overlying Proterozoic Elba Quartzite (Compton, 1975). The only remnants of the upper plate crop out as scattered klippen of Palaeozoic metasedimentary rocks in the eastern Raft River Mountains (Fig. 2; Compton, 1975; Wells, 1997, 2001; Wells *et al.* 1998).

2.b. The Raft River detachment shear zone

The Miocene Raft River detachment shear zone is localized within the Proterozoic Elba Quartzite (Fig. 2; Compton, 1972, 1975; Compton *et al.* 1977; Malavieille, 1987*a*; Wells, 2001; Sullivan, 2008; Gottardi & Teyssier, 2013). The basement shows little deformation, suggesting that the rheology contrast between the Elba Quartzite and basement facilitated strain localization, and the Elba Quartzite acted as a stress guide (Malavieille, 1987*a*; Wells, 2001; Sullivan, 2008; Gottardi & Teyssier, 2013).

The Elba Quartzite contains, from bottom to top, a basal quartzite-cobble metaconglomerate, an alternating sequence of white quartzite and muscovite-quartzite schist, a very distinctive layer of red quartzite and a sequence of alternating feldspar-rich micaceous quartzite, pure quartzite and pebble-gravel metaconglomerate (Fig. 2; Wells *et al.* 1998; Sullivan, 2008; Gottardi & Teyssier, 2013). Microstructural analysis combined with oxygen stable isotope geothermometry of quartz–muscovite pairs from the Elba Quartzite mylonite suggests that the Miocene Raft River detachment shear zone evolved under greenschist-facies

https://doi.org/10.1017/S0016756822000231 Published online by Cambridge University Press

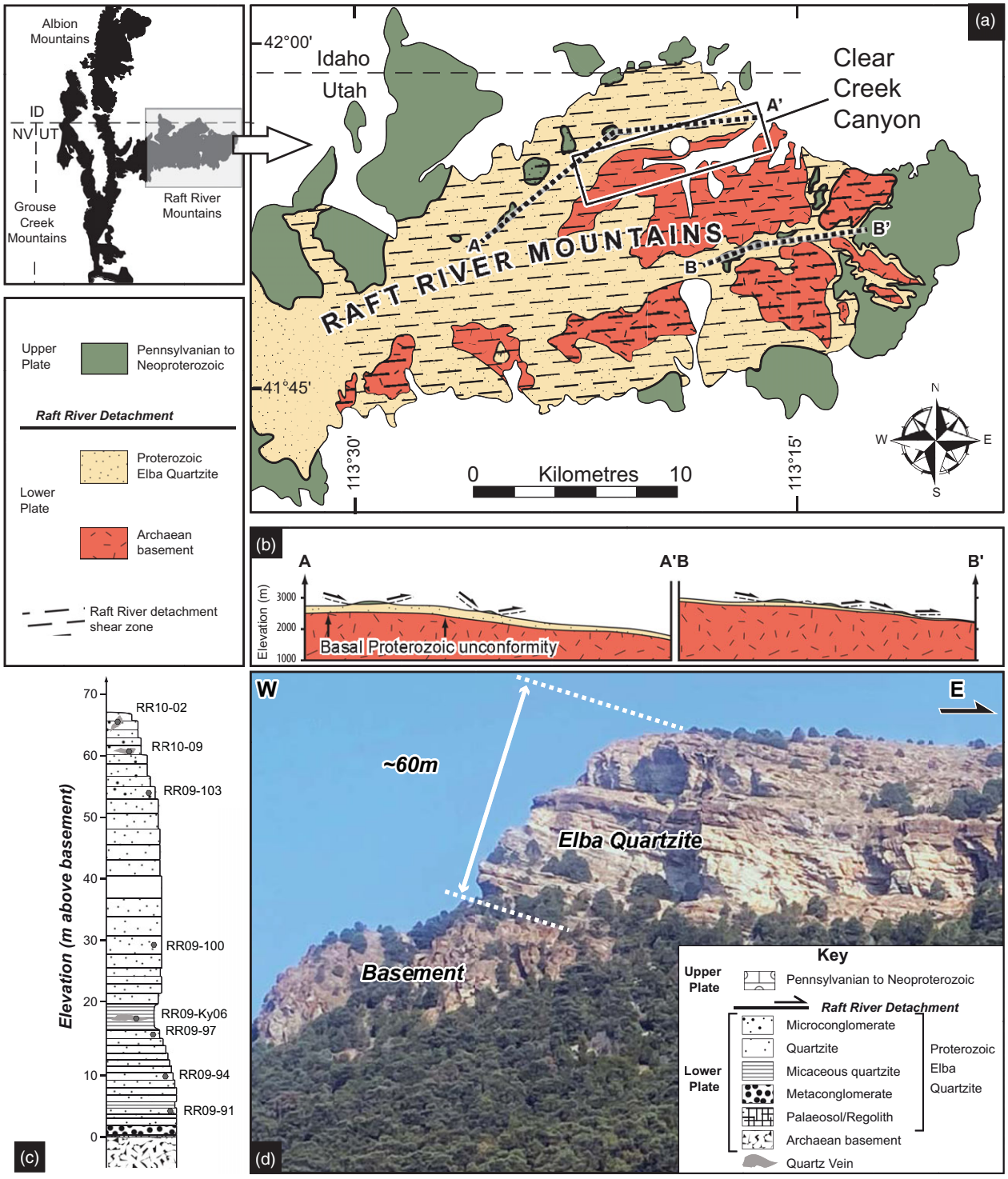

Fig. 2. Simplified regional geologic map of the eastern Raft River Mountains, with the location of the Clear Creek Canyon (study area). (a) Detailed map of the study area, the Clear Creek Canyon. White dot indicates location of collected samples. (b) Cross-section through the Raft River Mountains. Modified from Gottardi & Teyssier (2013) and Gottardi *et al.* (2015). (c) Vertical profile through the Raft River detachment shear zone. The ~50 to 75 m thick shear zone is localized in the Elba Quartzite. The Quartzite mylonite is composed of ~90 % quartz and ~10 % muscovite. (d) Picture of the Raft River Mountains detachment shear zone at Clear Creek Canyon.

conditions (~350–475 °C; Gottardi *et al.* 2011; Gottardi & Teyssier, 2013).

The mylonitic foliation, defined by flattened and elongated muscovite grains, is sub-horizontal, shallowly dipping to the east and follows the gentle domal shape of the core complex (Compton, 1980; Wells, 1997; Sullivan, 2008; Gottardi & Teyssier, 2013). The lineation, expressed by stretched muscovite grains on the foliation planes, clearly indicates a top-to-the-E sense of shear (Compton, 1980; Wells, 1997, Sullivan, 2008; Gottardi & Teyssier, 2013). Previous kinematic analyses of the Raft River detachment shear zone, including type-II S-C fabrics, asymmetric tails around feldspar porphyroclasts, shear bands, asymmetric quartz c-axis cross-girdles and single girdles

https://doi.org/10.1017/S0016756822000231 Published online by Cambridge University Press

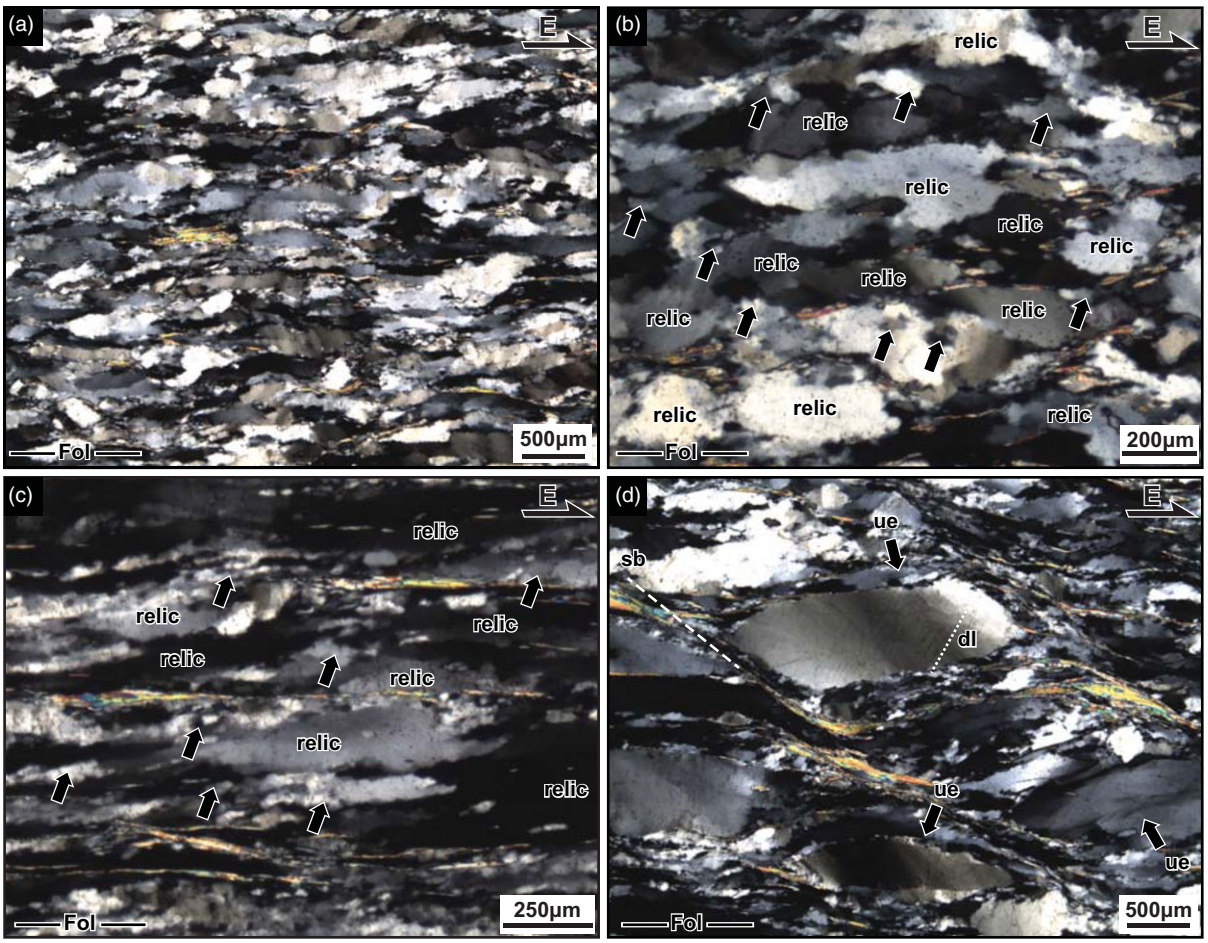

Fig. 3. Cross-polarized thin-section photomicrographs showing (a) representative quartz and muscovite microstructures of the Elba Quartzite mylonite from the Raft River detachment shear zone. (b, c) The quartz grain population is divided into large relict grains and small recrystallized grains (arrows). (d) Relict grains show strong undulose extinction (ue) and commonly contain deformation lamellae (dl). When present, shear bands (sb) form at a shallow angle (~10–20°) to the mylonitic foliation. Thin-sections cut perpendicular to foliation (fol) and parallel to lineation; the photomicrographs are taken oriented top-to-the-E.

all provide consistent evidence of a top-to-the-E sense of shear (Compton, 1980; Sabisky, 1985; Malavieille, 1987*a*,*b*; Wells, 1997, 2001; Sullivan, 2008; Gottardi *et al.* 2011, 2015; Gottardi & Teyssier, 2013).

3. Methodology

The samples investigated in this study were collected on a vertical transect across the Raft River detachment shear zone at Clear Creek Canyon. Six representative samples of the quartzite mylonite were analysed (Fig. 2). The detachment shear zone also hosts numerous quartz veins that are either transposed parallel to the foliation (samples RR09-Ky06 and RR10-02) or at a high angle to the foliation (sample RR10-09). Petrographic analysis was conducted on standard thin-sections (30 µm thick) prepared from eight quartzite mylonite samples collected across the Raft River detachment shear zone (Fig. 2c). Thin-sections were prepared from billets cut perpendicular to the mylonitic foliation and parallel to the lineation. Whole thin-section scans were acquired with a digital film scanner to gather plain- and crossed-polarized images in order to investigate the orientation of healed microfractures. Microstructural analysis was then conducted using a Nikon Eclipse LV100 microscope using 5×, 10×, 20× and 50× objectives and a 100× oil immersion objective to observe fluid inclusions. Using a Leitz Wetzlar 3-axis universal stage mounted to a Zeiss optical microscope, the orientation of intracrystalline fluid inclusion planes and their host quartz crystal c-axis were determined using 150 µm thick thin-sections of the same eight samples. The software ImageJ (Schneider *et al.* 2012) was used for measuring fluid inclusion plane orientation and fluid inclusion size. The software Orient (Vollmer, 2015) was used to plot stereographic projections of orientation data, such as fluid inclusion planes.

4. Results

We first present a microstructural analysis of the quartzite mylonite, then focus on the secondary fluid inclusions found in six quartzite mylonite samples collected across the detachment shear zone, and two quartz vein samples collected near the top of the detachment shear zone (Fig. 2c). Our results show that fluid inclusions are found in three types of microstructures: (1) healed microcracks, (2) transgranular fluid inclusion planes, and (3) grain boundary fluid inclusion clusters.

4.a. Microstructural analysis

The quartzite is characterized by two quartz grain populations: coarse elongate (>500 µm long) grains or 'relict' grains, and finer recrystallized grains (20–100 µm) (Fig. 3a–c). The relict grains have moderate to high aspect ratios (1:2 to 1:5) and define the

https://doi.org/10.1017/S0016756822000231 Published online by Cambridge University Press

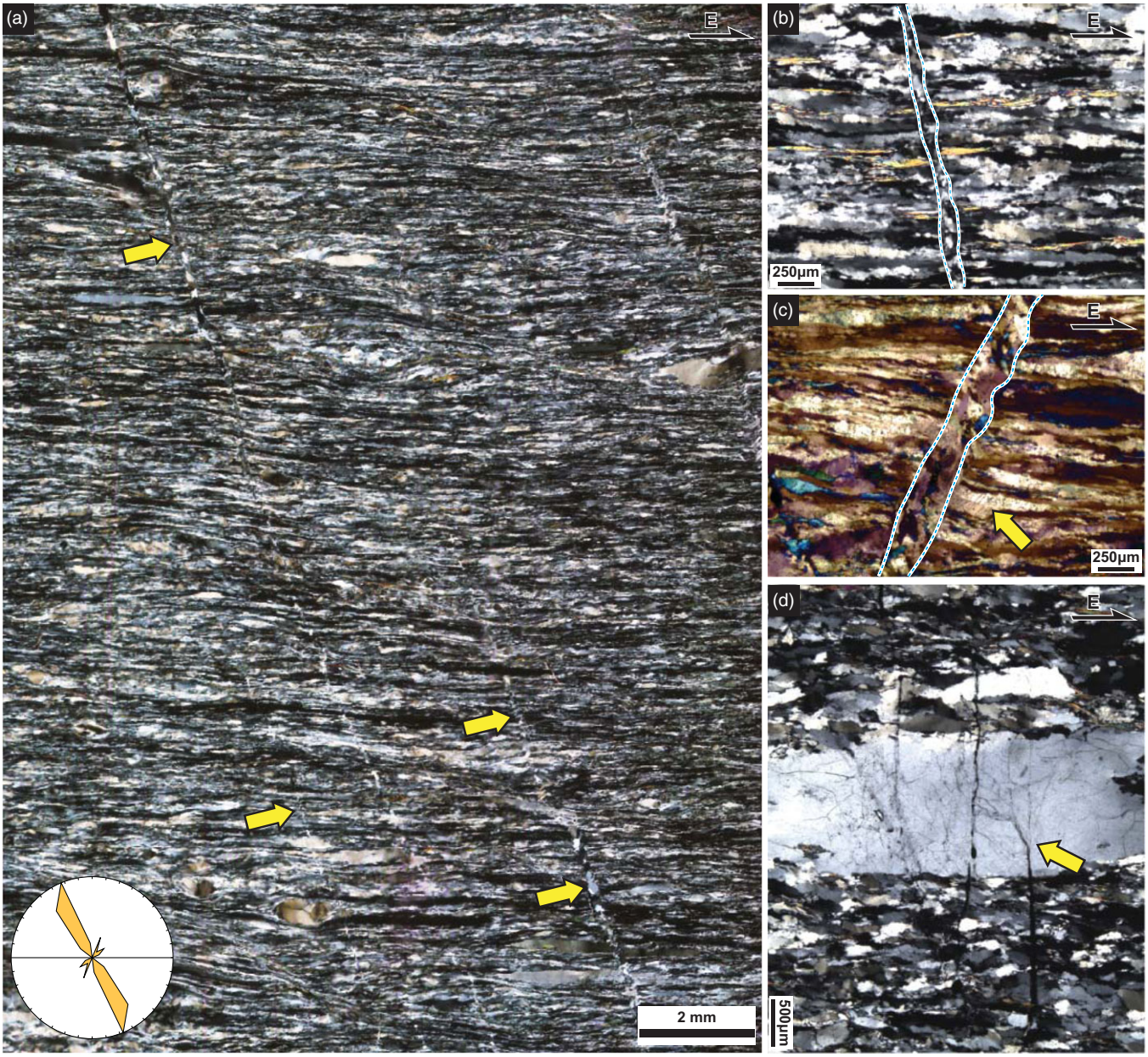

Fig. 4. Cross-polarized photomicrographs of thin-sections oriented perpendicular to the foliation and parallel to the lineation. (a–c) Microcracks tend to be oriented at a high angle to the mylonitic foliation (see circular frequency polygon). They are filled with quartz, which has a distinct fabric, not as strong as the mylonitic fabric, suggesting that microcracks healed while the shear zone was still at conditions favourable for quartz crystal plasticity. Fluid inclusions are abundant within the quartz fill and seem to be forming fluid inclusion planes that are sub-parallel with the walls of the microcracks (yellow arrow). (d) Horsetail structures (yellow arrow) are commonly found at the tip of mineralized microcracks. These structures contain a large number of fluid inclusion planes that typically fan out both upward and downward at the tip of the cracks.

macroscopic fabric. They typically exhibit strong undulose extinction, deformation bands and deformation lamellae (Fig. 3d). Recrystallized grains are found at the boundaries of relict grains (Fig. 3b, c). They are equant or blocky to slightly elongate and have a direct relation to subgrains present in large grains. Recrystallized grains locally form a low-angle oblique secondary foliation at 30–35° to the macroscopic foliation, indicating a top-to-the-E sense of shear, consistent with other kinematic criteria (Compton, 1980, Sullivan, 2008; Gottardi & Teyssier, 2013). Although not common, shear bands tend to form at a shallow angle (~10–20°) to the mylonitic foliation. Shear bands are typically associated with grain-size reduction. Relict grains in the vicinity of shear bands show an asymmetric shape and muscovite tails indicative of a top-to-the-E sense of shear.

Muscovite grains define the mylonitic foliation and typically pin relict quartz grains (Fig. 3c). Muscovite tends to form thin folia that rarely exceed a thickness of 50 μm. Muscovite grains also form two populations: large folia defining the foliation (Fig. 3c) and occasionally forming shear bands (Fig. 3d), and small, rhomb-shaped grains commonly found pinning quartz grains (Fig. 3b).

4.b. Fluid inclusions related to deformation fabrics

The distribution of fluid inclusions was observed in thin-sections oriented perpendicular to the foliation and parallel to the lineation (XZ). The nomenclature for describing fluid inclusions is defined by the physical and chemical properties of each inclusion (Kranz, 1983; Roedder, 1984; Lespinasse, 1999; Lespinasse *et al.* 2005).

https://doi.org/10.1017/S0016756822000231 Published online by Cambridge University Press

Fluid inclusions that define planar trails (fluid inclusion planes) are known as *secondary* fluid inclusions (Fig. 6). We observe secondary fluid inclusions that cross multiple grains, referred to as *transgranular*, and single grains, referred to as *intragranular*. Grain boundary fluid inclusions are also common in the studied samples. Although not observed in this study, the nomenclature for individual isolated fluid inclusions that formed coevally with either vein formation or host mineral crystallization are called *primary* fluid inclusions.

4.b.1. Healed microfractures

Healed microfractures are common structures found in all studied samples (Fig. 4). These through-going fractures cut across the entire thin-section (Fig. 4a). The fractures cut across the mylonitic foliation, and often offset muscovite grains (Fig. 4b). The width of the healed microfractures ranges from ~20 to 100 μm (Fig. 4b). The microfractures are filled with quartz, which has a fabric, not as strong as the fabric in adjacent quartz grains in the mylonite. Two adjacent microfractures sometimes exhibit stepover patterns. Fluid inclusions are abundant in the vicinity of the healed microfractures, typically occurring in planes parallel to the microfracture (Fig. 4c). The tip of the microfractures is commonly accompanied by horsetail structures that fan out both upward and downward (Fig. 4d). Fluid inclusions are particularly abundant in the horsetail fractures and follow the offshoot fractures (Fig. 4d). The dip of the healed microfracture was measured with respect to the mylonitic foliation in the XZ plane of each thin-section (Fig. 5a). Three sets have been identified: a conjugate set that is oriented at ~30° ± 10° and ~130° ± 10° clockwise from the mylonitic foliation, and a set that is sub-perpendicular to the mylonitic foliation (Fig. 5).

4.b.2. Transgranular fluid inclusion planes

Fluid inclusion planes cross multiple grains (transgranular) and single grains and subgrain boundaries (intergranular). Transgranular fluid inclusion planes tend to group in multiple parallel sets rather than be isolated (Fig. 6a, b). The orientation of these transgranular fluid inclusion planes is somewhat similar to the healed microcracks: in boudinaged vein samples collected near the top of the detachment shear zone, transgranular fluid inclusion planes are oriented sub-perpendicular to the mylonitic foliation (Fig. 6a). In the quartzite mylonite samples, the transgranular fluid inclusion planes occur in two conjugate orientations, dipping at ~40° ± 10° and 135° ± 10° measured clockwise from the mylonitic foliation (Figs 5b, 6b), an orientation similar to the conjugate sets of healed microfractures. These transgranular fluid inclusion planes typically cut across multiple elongate relict quartz grains that define the mylonitic foliation and can be hundreds of microns long. Conjugate sets of fluid inclusions commonly cross-cut each other (Fig. 6b). Transgranular planes typically preserve a high number (100–1000s) of fluid inclusions.

Fluid inclusion planes are predominantly found to be populated by small circular 1–3 μm single-phase inclusions within mylonite (Figs 7, 8). Many of these inclusions have dark rims that could indicate possible trapped high-density fluids (Fig. 8a). Isolated inclusions are multi-phased at room temperature and are typically characterized by a vapour and liquid component (Fig. 8b).

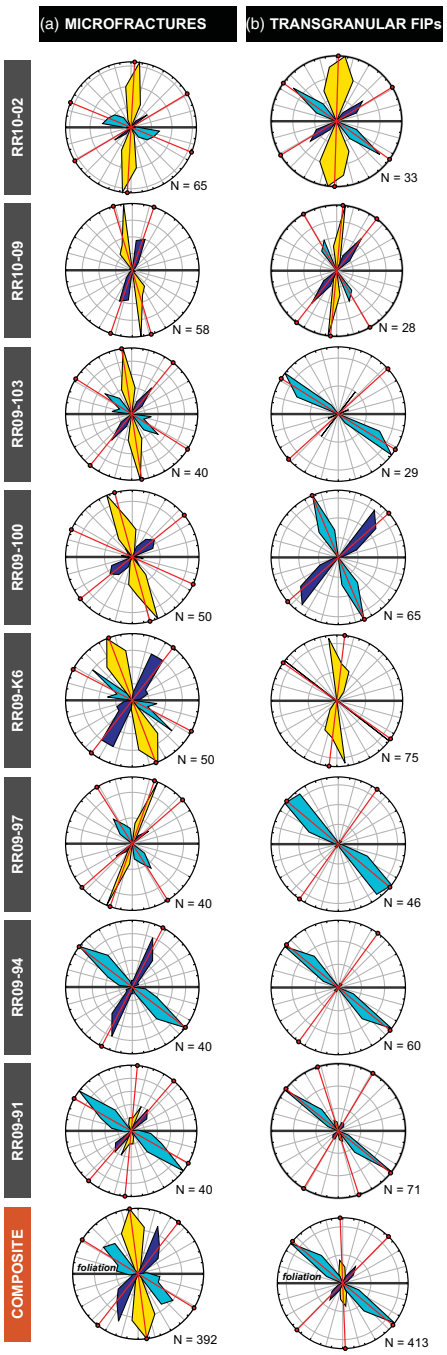

Fig. 5. Orientations of (a) healed microfractures and (b) transgranular fluid inclusion planes (FIPs) within both mylonite and quartz vein samples. Frequency polygons of each sample and the composite frequency polygon show three sets of healed microfractures: one set sub-perpendicular to the mylonitic foliation (yellow) and two conjugate sets. The conjugate sets are oriented ~30° ± 10° (light blue) and ~130° ± 10° (dark blue) for the microfractures, and ~40° ± 10° (light blue) and ~135° ± 10° for the transgranular fluid inclusion planes, clockwise with respect to the mylonitic foliation (central black line on the frequency polygon, labelled on the composite diagram). The red line on the frequency polygon indicates the average of the specific cluster. The block diagram represents the schematic orientation of these three sets of healed microfractures with respect to the mylonitic fabric. See Figure 2c for sample location.

https://doi.org/10.1017/S0016756822000231 Published online by Cambridge University Press

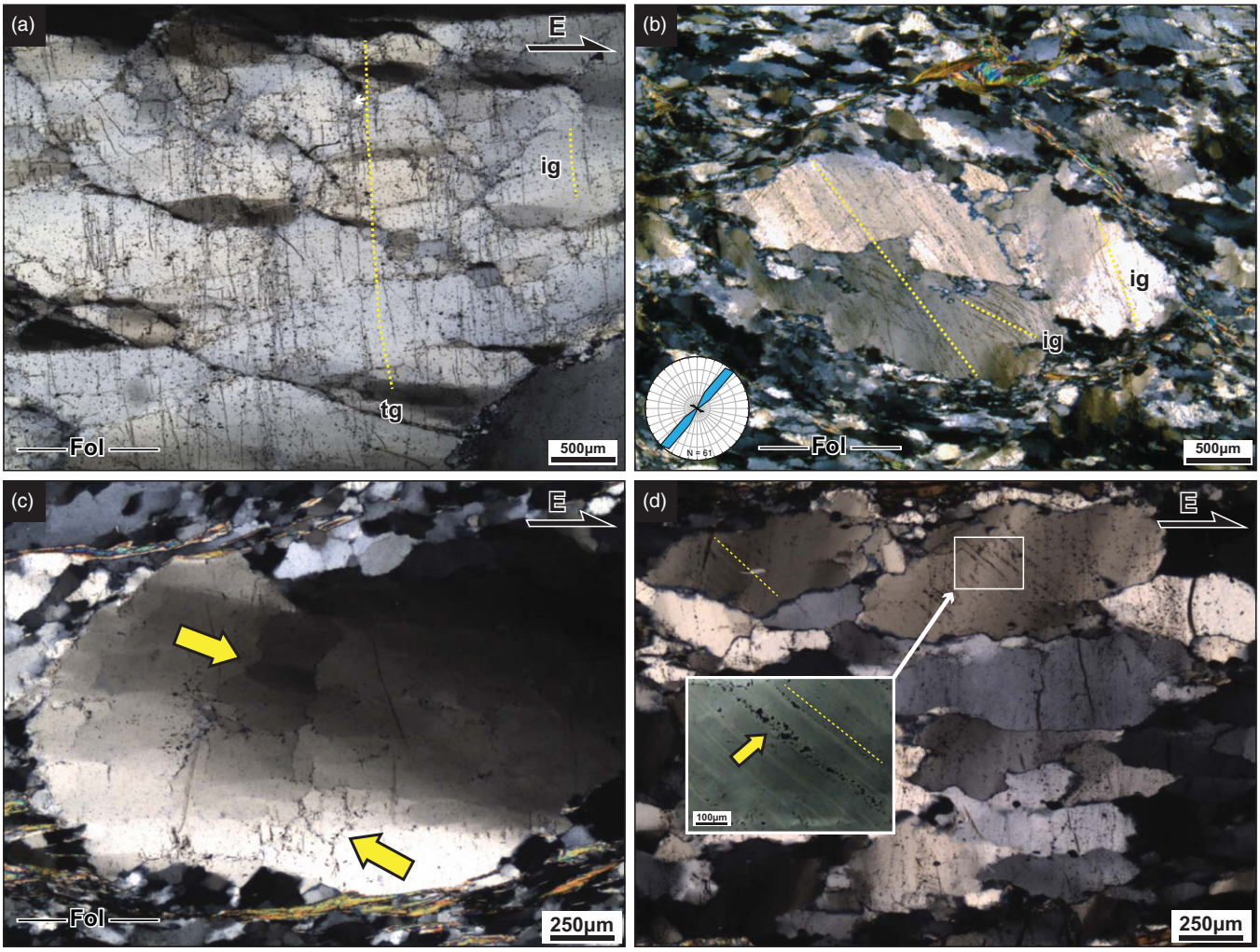

Fig. 6. Cross-polarized photomicrographs of thin-sections oriented perpendicular to the foliation and parallel to the lineation. Fluid inclusion planes cross multiple grains (transgranular, tg) and single grains and subgrain boundaries (intergranular, ig). (a) In boudinaged vein samples collected near the top of the detachment shear zone, transgranular fluid inclusion planes are oriented sub-perpendicular to the mylonitic foliation (Fol). (b) In quartzite mylonite samples collected at deeper structural levels, the transgranular fluid inclusion planes occur in two conjugate orientations, dipping at ~40–60° from the mylonitic foliation. These transgranular fluid inclusion planes typically cut across elongate relict quartz grains that define the mylonitic foliation and can be hundreds of microns long. Individual fluid inclusion planes (FIP) typically preserve a high number of fluid inclusions. (c) Grain boundary fluid inclusions are common in the quartzite mylonite. They are either found around recrystallized quartz grains or they outline subgrain boundaries in large relict grains (yellow arrows). (d) Deformation lamellae are found in 20–50 % of quartz grains in the quartzite mylonite (dashed yellow lines). They are very well developed in large quartz grains that are elongated at a high angle to foliation but occur also in smaller recrystallized grains. Deformation lamellae are commonly decorated by fluid inclusions (yellow arrow).

Larger inclusions commonly exhibit three phases (Fig. 8c). These triphase inclusions are composed of the typical vapour and liquid components but exhibit a euhedral solid crystal overlying the top section of the inclusion (Fig. 8c).

4.b.3. Grain boundary fluid inclusions

Grain boundary fluid inclusions and clusters of intragranular fluid inclusions are common in all studied quartzite mylonite samples, rare in the boudinaged vein samples. They are common around recrystallized quartz grains and typically outline subgrain boundaries in large relict grains (Fig. 6c). They form dense clusters at grain boundaries. When inclusions are trapped within the interior of a relic, they form clusters that are sub-planar, oriented sub-perpendicular to transgranular fluid inclusion planes.

Lastly, fluid inclusions are particularly abundant in quartz deformation lamellae (Fig. 6d). Deformation lamellae are found in 20–50 % of quartz grains in the quartzite mylonite. They are very well developed in large relict quartz grains that are elongated at a high angle to foliation but occur also in smaller recrystallized grains. Deformation lamellae are commonly decorated by fluid inclusions. Deformation lamellae and fluid inclusion planes usually have a similar orientation.

4.c. Quartz c-axis orientation

The orientations of intracrystalline fluid inclusion planes and their host quartz crystal c-axes were measured using a universal stage mounted on an optical microscope. Results gathered with the universal stage were plotted on equal-area, lower-hemisphere stereographic projections (Fig. 9; Table 1). For both the quartzite mylonite and quartz vein samples, quartz c-axes cluster in the centre of the stereonet, forming a point distribution. The trend

https://doi.org/10.1017/S0016756822000231 Published online by Cambridge University Press

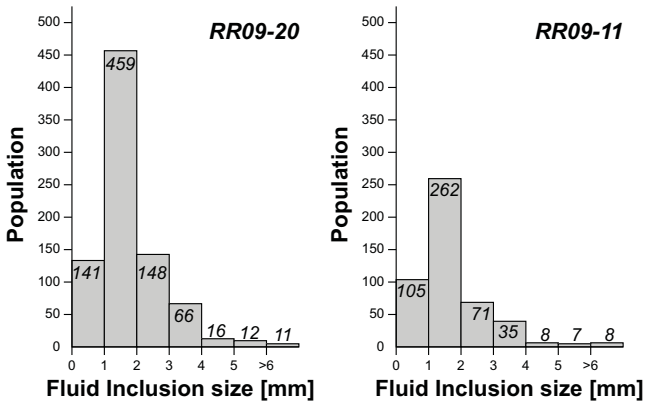

Fig. 7. Histogram of transgranular fluid inclusion size distribution for two samples. Average inclusion size in most samples averages around 1.8 µm.

and plunge of quartz c-axes ranges from 351° to 14° and 63° to 74°, with an average of 4° ± 10° and 69° ± 2°. These results indicate that the measured quartz grains are oriented such that their c-axes are contained within the foliation plane, and oriented perpendicular to the lineation. This orientation is consistent with quartz dynamic recrystallization by prism <a> slip.

The orientation of the fluid inclusion planes within the measured quartz grains is also very consistent across all samples. The strike and dip of the fluid inclusion planes range from 48° to 98° and 10° to 17°, with an average of 82° ± 12° and 26° ± 2°. These results indicate that the fluid inclusion planes are oriented sub-parallel to the basal crystallographic planes of quartz (Fig. 9), perpendicular to the foliation and parallel to the lineation.

5. Discussion

5.a. Deformation mechanisms

The crystal-plastic and brittle microstructural record of the quartzite mylonite from the Raft River detachment shear zone provides insight into fluid circulation during exhumation of the shear zone. Microstructures indicate that quartz deformed primarily by dislocation creep, subgrain rotation and minor grain boundary migration recrystallization (Fig. 3; Regime II of Hirth & Tullis, 1992), suggesting deformation temperatures of 450–500 °C (Stipp *et al.* 2002). This temperature range is probably related to the latest stages of crystal-plastic deformation of quartz, because the majority of relict quartz grains exhibit microstructures such as relict quartz grains with undulose extinction and deformation lamellae, that are all evidence of high-stress/high-strain rate deformation conditions (Fig. 3d), indicating that deformation was occurring close to the brittle–ductile transition. In particular, deformation lamellae have been interpreted to reflect plastic high-stress deformation in alloys and metals (Drury, 1993), and short-term plastic and eventually brittle deformation related to coseismic loading in rocks (Trepmann & Stöckhert, 2003; Trepmann & Seybold, 2019). Deformation lamellae were preserved owing to a lack of recovery during deformation, suggesting that recovery in the quartzite was not efficient enough to keep up with strain rate and offset strain hardening (e.g. Gottardi & Teyssier, 2013). These observations suggest that during the latest stages of exhumation, the detachment system evolved close to the brittle–ductile transition, switching back and forth between dislocation creep and glide-controlled exponential creep, depending on the temperature/strain-rate/fluid conditions (Gottardi & Teyssier, 2013).

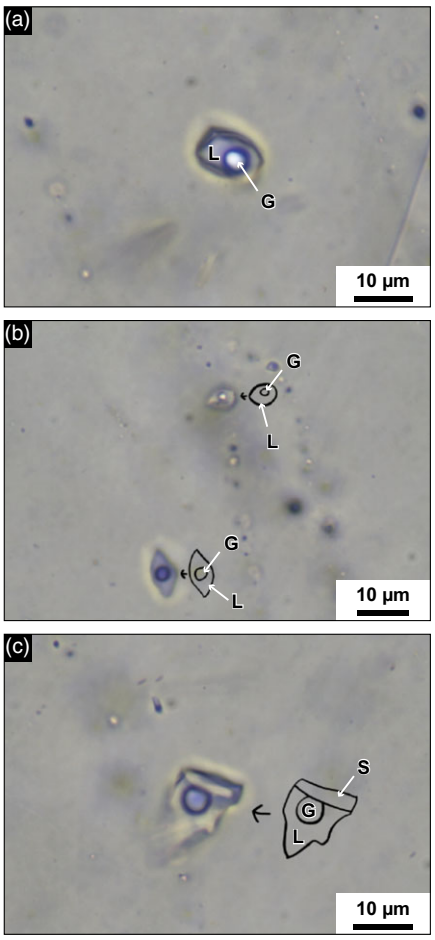

Fig. 8. Plain-polarized photomicrographs of thin-sections oriented perpendicular to the foliation and parallel to the lineation. (a) Inclusion with dark rims, possibly indicative of high-density fluid. (b) Photomicrograph of a two-phase fluid inclusion with large inner phase that is stationary. (c) Photomicrograph of a three-phase fluid inclusion that has stationary inner phases. L – liquid; G – gas (vapour bubble); S – solid.

The mylonitic fabric is overprinted by several brittle structures: healed microfractures and transgranular fluid inclusions planes (Figs 4, 6). Both of these structures occur in similar orientations: one is sub-perpendicular to the mylonitic foliation, and a conjugate set occurs oriented at ~35° ± 10° and ~135° ± 10° clockwise from the mylonitic foliation (Fig. 10). These two different orientations may be caused by a minor switch in the stress field during exhumation of the detachment shear zone. Healed microfractures and transgranular fluid inclusion planes are consistent in orientation across all studied samples (Fig. 5). The orientation of these structures is consistent with the E-directed shear kinematics preserved in plastically deformed footwall mylonite, such as type-II S-C fabrics, asymmetric tails around feldspar porphyroclasts, shear bands and asymmetric quartz c-axis cross-girdles (Wells, 1997; Sullivan, 2008; Gottardi & Teyssier, 2013).

5.b. Condition of fluid entrapment

The oxygen and hydrogen stable isotope geochemistry of quartz, muscovite and fluid inclusions from the quartzite mylonite suggests that meteoric fluid infiltration occurred during the

https://doi.org/10.1017/S0016756822000231 Published online by Cambridge University Press

Table 1. Fisher spherical vector mean orientation of host quartz c-axis and respective fluid inclusion planes, with a 95 % confidence error

Sample no.	c-axis				Fluid inclusion plane			
	Trend		Plunge		Strike		Dip	
Quartzite mylonite								
91–02 (N = 30)	6	±13	69	±2	48	±23	25	±2
91–03 (N = 31)	14	±11	70	±2	69	±13	28	±1
91–06 (N = 30)	351	±12	74	±3	89	±11	27	±2
91–08 (N = 30)	5	±9	69	±2	86	±14	25	±2
91–09 (N = 30)	3	±12	70	±2	94	±14	28	±2
91–10 (N = 30)	359	±11	71	±3	81	±15	27	±2
Average	**3**	**±11**	**70**	**±2**	**78**	**±15**	**27**	**±2**
Quartz veins								
10–02 (N = 20)	8	±16	65	±3	89	±17	22	±2
10–09 (N = 20)	9	±12	64	±3	98	±12	28	±2
Average	**8**	**±14**	**64**	**±3**	**93**	**±14**	**25**	**±2**

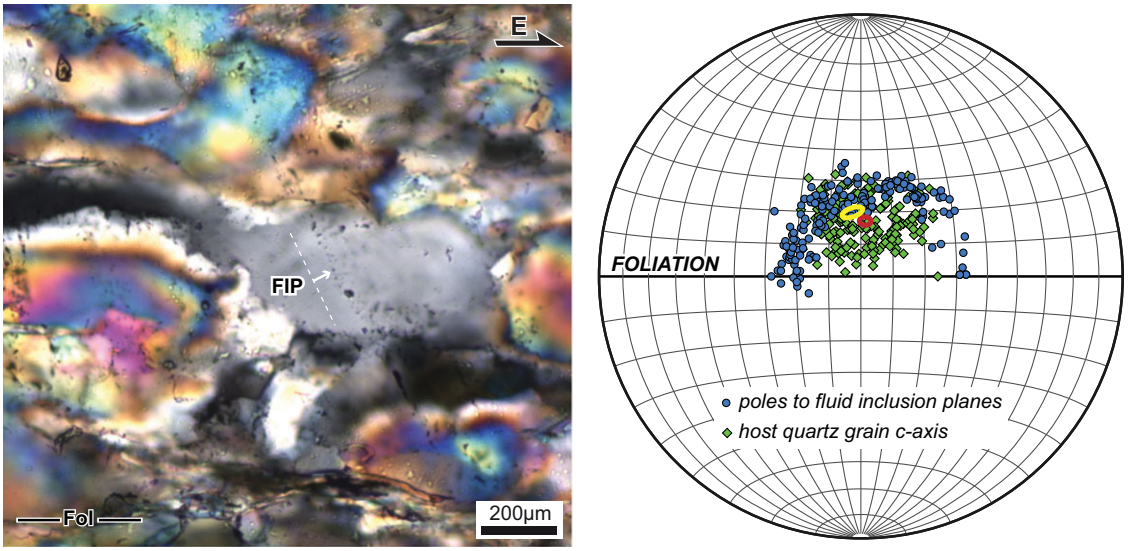

Fig. 9. (Left) Cross-polarized photomicrograph of the quartzite mylonite showing quartz grain (grey, in the centre of the image) with fluid inclusion plane (FIP). (Right) Equal-area, lower-hemisphere stereographic projections of the orientation of poles to planes of intragranular fluid inclusions and host quartz c-axes, measured with respect to the mylonitic foliation.

Miocene extension and exhumation of the Raft River detachment shear zone (Gottardi *et al.* 2011, 2015; Methner *et al.* 2015). Oxygen isotope geothermometry of quartz and syn-kinematic muscovite indicates that Miocene deformation by dynamic recrystallization of quartz and muscovite occurred at a temperature of 350–485 °C (Gottardi *et al.* 2011, 2015). The hydrogen isotope signatures of fluid inclusions (−94 ‰ to −82 ‰) and fabric-forming recrystallized muscovite (−120 ‰ to −90 ‰) demonstrate that meteoric fluids infiltrated the shear zone during the Miocene deformation event (Gottardi *et al.* 2011, 2015).

The microstructural observations indicate that trapping conditions of the fluid likely occurred during coeval brittle and plastic deformation of quartz, but before complete cooling of the footwall rocks. The fact the quartz grains filling the microfractures have a preferred orientation and show evidence of subgrain rotation recrystallization (Fig. 4) suggests that the temperature was still above ~400 °C when the microfractures healed. Altogether, these microstructural observations suggest that brittle–ductile processes that allowed fluid flow and the trapping of fluid inclusions must have occurred between the latest stage of crystal-plastic deformation and before the complete exhumation and cooling of the footwall rocks.

5.c. Model for fluid circulation

The microstructural record preserved in the quartzite mylonite of the Raft River detachment shear zone correlates to rapid exhumation of hot mid- to lower crustal rocks that can drive fluid circulation and heat advection into the upper crust (Morrison & Anderson, 1998; Gottardi *et al.* 2011; Siebenaller *et al.* 2013, 2016;

https://doi.org/10.1017/S0016756822000231 Published online by Cambridge University Press

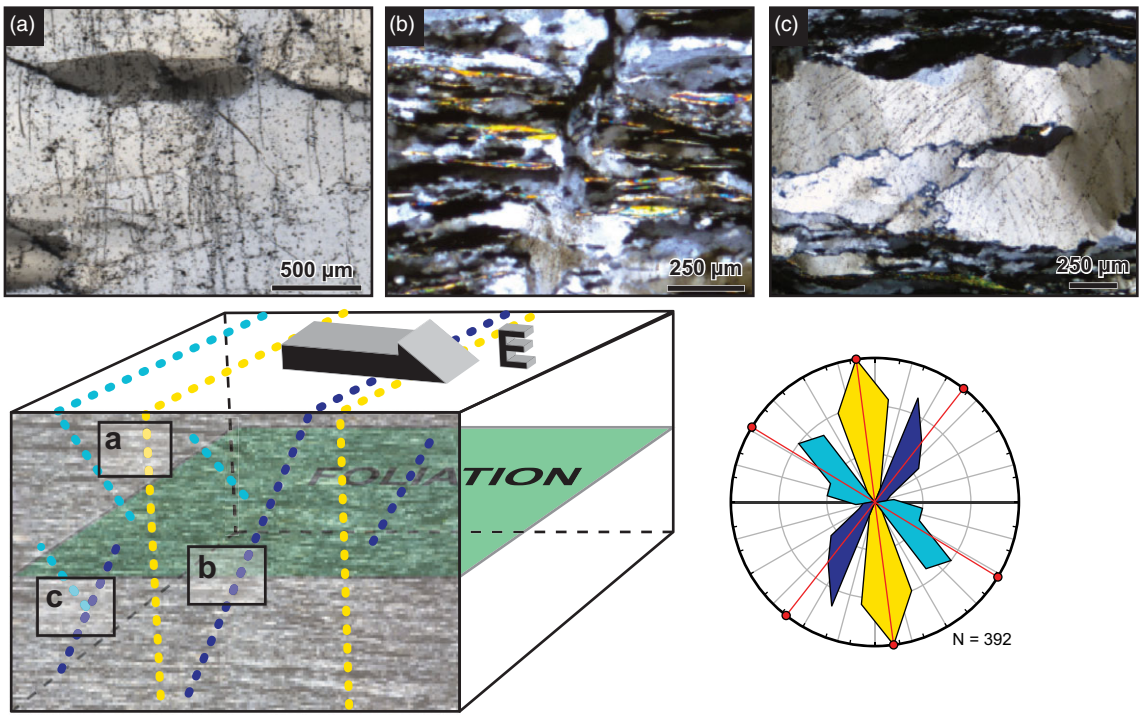

Fig. 10. Composite frequency polygon and block diagram representing the general orientation of brittle microstructures (healed microfractures and transgranular fluid inclusion planes) with respect to the mylonitic foliation and lineation.

Carter *et al.* 2015; Quilichini *et al.* 2015; Ceccato *et al.* 2017; Compton *et al.* 2017; Dusséaux *et al.* 2019; Marchesini *et al.* 2019; Prando *et al.* 2020; Menegon & Fagereng, 2021). Our results show that both crystal-plastic and brittle deformation mechanisms affected the detachment shear zone at the time of fluid inclusion entrapment (Figs 4, 6). These results suggest that brittle fractures, such as normal faults and healed microcracks, are important structures for fluid transfer in metamorphic core complexes and extending crustal rocks in general (e.g. López *et al.* 1994; Sibson, 2000).

Based on our microstructural observation, we propose the following mechanism for meteoric fluid infiltration in the deforming shear zone. Abundant evidence of high-stress plastic deformation in the detachment shear zone suggests that the response of the quartzite mylonite to stress hardening is seismic failure (Fig. 11). When the detachment shear zone is still at depth, a ~400–500 °C temperature allows quartz deformation by dislocation creep processes such as subgrain rotation (Figs 3, 11a). However, owing to high differential stress, dislocation creep cannot keep up with either a fast strain rate or strain hardening, leading to high-stress plasticity features such as undulose extinction and deformation lamellae (Fig. 6d). Eventually, stress build-up leads to embrittlement and brittle failure. Brittle failure leads to the formation of faults, fractures and microcracks, which allow for surface fluids to be pumped into the shear zone (Fig. 11b; Sibson, 1977; McCaig, 1988; Lister & Davis, 1989; Carter *et al.* 2015; Siebenaller *et al.* 2016; Compton *et al.* 2017; Prando *et al.* 2020; Menegon & Fagereng, 2021). After rupture, during post-seismic relaxation, stress decays and the detachment shear zone re-enters the dislocation creep regime. Microfractures heal, as indicated by the fabric preserved in the quartz fill, thereby trapping fluid inclusions (Figs 4, 6, 11c). The intragranular fluid inclusion planes and subgrain boundary fluid inclusions likely represent the remnants of some former brittle fluid inclusion plane reworked by the cyclical ductile shearing. Additional stress build-up likely expelled large fluid inclusions from the fluid inclusion planes and broke them down into smaller inclusions (>1 µm). Crystal-plastic deformation by subgrain rotation and grain boundary migration eventually redistributes these small inclusions as grain and subgrain boundary fluid inclusion clusters (Fig. 11). These tight clusters of small fluid inclusions (>1 µm) typically indicate that explosion of larger inclusions was likely caused by isobaric heating or decompression forces during tectonic processes (Vityk & Bodnar, 1995). This cycle likely repeated several times during the exhumation of the detachment shear zone.

6. Conclusions

Microstructural analysis of samples of quartzite mylonite from the Raft River detachment shear zone provides insight into meteoric fluid infiltration near the brittle–ductile transition during progressive exhumation of the shear zone. Our microstructural observation reveals the presence of several fluid-related microstructures: healed microcracks, transgranular fluid inclusion planes and grain boundary fluid inclusion clusters. The presence of fluid-related microstructures, in combination with high-stress/high-strain rate microstructures such as deformation lamellae and undulose extinction, suggest that the detachment shear zone evolved close to the brittle–ductile transition. Healed microcracks and transgranular fluid inclusion planes occur in three sets, one sub-perpendicular to the mylonitic foliation, and a conjugate set oriented at ~40–60° to the mylonitic foliation. Healed microfractures are filled with quartz, which has a distinct fabric, not as strong as the mylonitic fabric, suggesting that microcracks healed while the shear zone was still at conditions favourable for quartz crystal plasticity. Fluid inclusions also commonly

https://doi.org/10.1017/S0016756822000231 Published online by Cambridge University Press

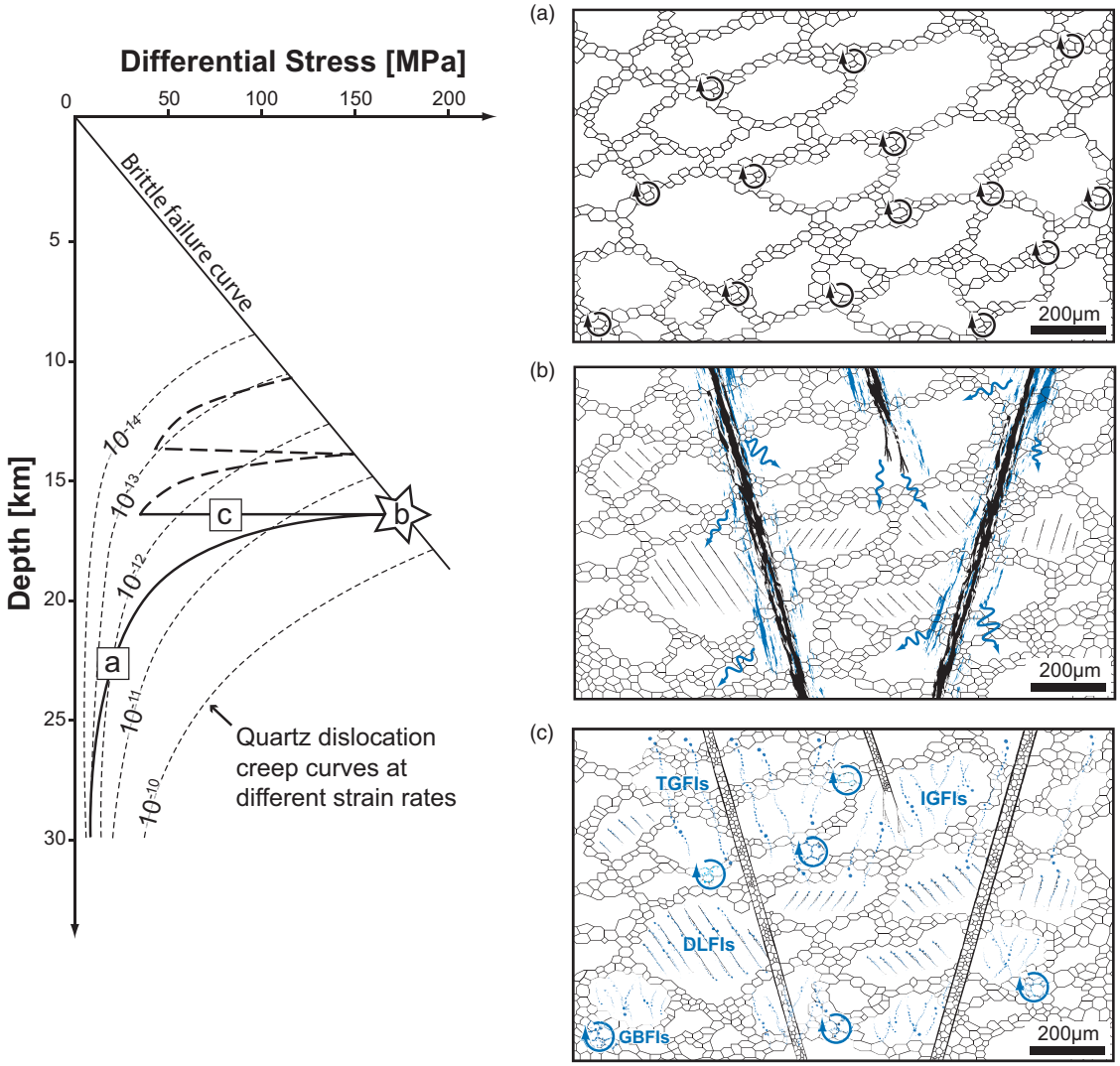

Fig. 11. Model for fluid circulation based on the various fluid-related microstructures observed in the Raft River detachment shear zone. Crustal strength profile of the continental crust, using Byerlee's law (Sibson, 1974) for the brittle upper crust and the Hirth *et al.* (2001) quartzite dislocation creep flow law for the lower crust. (a), (b), (c) show potential differential stress pathways for the observed microstructures. (a) During stress build-up, deformation of the quartz grain is accommodated by dislocation creep subgrain rotation recrystallization. (b) Strain hardening leads to embrittlement and eventually seismic brittle failure, forming faults, fractures and microcracks, which allow for surface fluids to be pumped into the shear zone. (c) Post-seismic relaxation heals fractures and traps the fluids as transgranular fluid inclusions (TGFIs) and intergranular fluid inclusions (IGFIs). Continued crystal-plastic deformation by subgrain rotation and grain boundary migration redistributes small fluid inclusions as grain/subgrain boundary fluid inclusion clusters (GBFIs).

decorate grain and subgrain boundaries as inter- and intragranular clusters. Our results show ductile overprint of brittle microstructures, which suggests that, during exhumation, the detachment shear zone may have crossed the brittle–ductile transition repeatedly, providing opportunities for fluid to permeate the detachment shear zone.

Acknowledgements. We gratefully acknowledge research support from the US National Science Foundation (EAR-184912) to RG. The authors thank Hannah Riegel and an anonymous reviewer for constructive reviews, and Olivier Lacombe for handling of the manuscript.

References

Armstrong RL (1968) Mantled gneiss domes in the Albion Range, Southern Idaho. *Geological Society of America Bulletin* **79**, 1295–314. doi: 10.1130/0016-7606(1968)79[1295:mgdita]2.0.co;2.

Armstrong RL and Hills F (1967) Rubidium-strontium and potassium-argon geochronologic studies of mantled gneiss domes, Albion Range, southern Idaho, USA. *Earth and Planetary Science Letters* **3**, 114–24. doi: 10.1016/0012-821x(67)90021-0.

Caine JS, Evans JP and Forster CB (1996) Fault zone architecture and permeability structure. *Geology* **24**, 1025–8.

Carter MJ, Siebenaller L and Teyssier C (2015) Orientation, composition, and entrapment conditions of fluid inclusions in the footwall of the northern Snake Range detachment, Nevada. *Journal of Structural Geology* **81**, 106–24.

Ceccato A, Pennacchioni G, Menegon L and Bestmann M (2017) Crystallographic control and texture inheritance during mylonitization of coarse grained quartz veins. *Lithos* **290**, 210–27.

Compton RR (1972) *Geologic Map of Yost Quadrangle, Box Elder County, Utah, and Cassia County, Idaho*. US Geological Survey Miscellaneous Geologic Investigations Map I-672, Scale 1:31 680. doi: 10.3133/i672.

Compton RR (1975) *Geologic Map of Park Valley Quadrangle, Box Elder County, Utah, and Cassia County, Idaho*. US Geological Survey Miscellaneous Geologic Investigations Map I-873, Scale 1:31 680. doi: 10.3133/i873.

https://doi.org/10.1017/S0016756822000231 Published online by Cambridge University Press

Compton RR (1980) Fabrics and strains in quartzites of a metamorphic core complex, Raft River Mountains, Utah. In *Cordilleran Metamorphic Core Complexes* (eds MD Crittenden, PJ Coney and GH Davis), pp. 385–98. Geological Society of America Memoir vol. 153. doi: 10.1130/mem153-p385.

Compton KE, Kirkpatrick JD and Holk GJ (2017) Cyclical shear fracture and viscous flow during transitional ductile-brittle deformation in the Saddlebag Lake Shear Zone, California. *Tectonophysics* **708**, 1–14.

Compton RR, Todd VR, Zartman RE and Naeser CW (1977) Oligocene and Miocene metamorphism, folding, and low-angle faulting in northwestern Utah. *Geological Society of America Bulletin* **88**, 1237–50. doi: 10.1130/0016-7606(1977)88<1237:oammfa>2.0.co;2.

Connolly JAD and Podladchikov YY (2004) Fluid flow in compressive tectonic settings: implications for midcrustal seismic reflectors and downward fluid migration. *Journal of Geophysical Research: Solid Earth* **109**, B04201. doi: 10.1029/2003JB002822.

Cox SF (2010) The application of failure mode diagrams for exploring the roles of fluid pressure and stress states in controlling styles of fracture-controlled permeability enhancement in faults and shear zones. *Geofluids* **10**, 217–33.

Dobe R, Das A, Mukherjee R and Gupta S (2021) Evaluation of grain boundaries as percolation pathways in quartz-rich continental crust using Atomic Force Microscopy. *Scientific Reports* **11**, 9831. doi: 10.1038/s41598-021-89250-z.

Drury MR (1993) Deformation lamellae in materials and minerals. In *Defects and Processes in the Solid State: Geosciences Applications: The McLaren Volume* (eds JN Noland and JD Fitz Gerald), pp. 195–212. Amsterdam: Elsevier Science Publishers.

Dusséaux C, Gébelin A, Boulvais P, Gardien V, Grimes S and Mulch A (2019) Meteoric fluid-rock interaction in Variscan shear zones. *Terra Nova* **31**, 366–72.

Famin V, Hébert R, Philippot P and Jolivet L (2005) Ion probe and fluid inclusion evidence for co-seismic fluid infiltration in a crustal detachment. *Contributions to Mineralogy and Petrology* **150**, 354–67.

Famin V, Philippot P, Jolivet L and Agard P (2004) Evolution of hydrothermal regime along a crustal shear zone, Tinos Island, Greece. *Tectonics* **23**, TC5004. doi: 10.1029/2003TC001509.

Ferry JM (1994) A historical review of metamorphic fluid flow. *Journal of Geophysical Research: Solid Earth* **99**, 15487–98.

Fusseis F, Regenauer-Lieb K, Liu J, Hough RM and De Carlo F (2009) Creep cavitation can establish a dynamic granular fluid pump in ductile shear zones. *Nature* **459**, 974–7.

Gilgannon J, Poulet T, Berger A, Barnhoorn A and Herwegh M (2020) Dynamic recrystallization can produce porosity in shear zones. *Geophysical Research Letters* **47**, e2019GL086172. doi: 10.1029/2019GL086172.

Gottardi R, Schaper MC, Barnes JD and Heizler MT (2018) Fluid–rock interaction and strain localization in the Picacho Mountains detachment shear zone, Arizona, USA. *Tectonics* **37**, 3244–60. doi: 10.1029/2017tc004835.

Gottardi R and Teyssier C (2013) Thermomechanics of an extensional shear zone, Raft River metamorphic core complex, NW Utah. *Journal of Structural Geology* **53**, 54–69. doi: 10.1016/j.jsg.2013.05.012.

Gottardi R, Teyssier C, Mulch A, Valley JW, Spicuzza MJ, Vennemann TW and Heizler M (2015) Strain and permeability gradients traced by stable isotope exchange in the Raft River detachment shear zone, Utah. *Journal of Structural Geology* **71**, 41–57. doi: 10.1016/j.jsg.2014.10.005.

Gottardi R, Teyssier C, Mulch A, Vennemann TW and Wells ML (2011) Preservation of an extreme transient geotherm in the Raft River detachment shear zone. *Geology* **39**, 759–62. doi: 10.1130/g31834.1.

Griggs D (1967) Hydrolytic weakening of quartz and other silicates. *Geophysical Journal International* **14**, 19–31.

Harris CR, Hoisch TD and Wells ML (2007) Construction of a composite pressure–temperature path: revealing the synorogenic burial and exhumation history of the Sevier hinterland, USA. *Journal of Metamorphic Geology* **25**, 915–34.

Hirschmann MM (2006) Water, melting, and the deep Earth H_2O cycle. *Annual Review of Earth and Planetary Sciences* **34**, 629–53.

Hirth G, Teyssier C and Dunlap JW (2001) An evaluation of quartzite flow laws based on comparisons between experimentally and naturally deformed rocks. *International Journal of Earth Sciences* **90**, 77–87.

Hirth G and Tullis J (1992) Dislocation creep regimes in quartz aggregates. *Journal of Structural Geology* **14**, 145–59. doi: 10.1016/0191-8141(92)90053-y.

Hoisch TD, Wells ML and Hanson LM (2002) Pressure-temperature paths from garnet-zoning: evidence for multiple episodes of thrust burial in the hinterland of the Sevier orogenic belt. *American Mineralogist* **87**, 115–31.

Kranz RL (1983) Microcracks in rocks: a review. *Tectonophysics* **100**, 449–80.

Lespinasse M (1999) Are fluid inclusion planes useful in structural geology? *Journal of Structural Geology* **21**, 1237–43.

Lespinasse M, Desindes L, Fratczak P and Petrov A (2005) Microfissural mapping of natural cracks in rocks: implications for fluid transfers quantification in the crust. *Chemical Geology* **223**, 170–8.

Lister GS and Davis GA (1989) The origin of metamorphic core complexes and detachment faults formed during Tertiary continental extension in the northern Colorado River region, USA. *Journal of Structural Geology* **11**, 65–94.

López DL, Smith L and Storey ML (1994) Modeling fluid flow and heat transfer at Basin and Range faults: preliminary results for Leach Hot Springs, Nevada. Restructuring the Geothermal Industry 18, 11–16.

Malavieille J (1987a) Extensional shearing deformation and kilometer-scale "a"- type folds in a Cordilleran Metamorphic Core Complex (Raft River Mountains, northwestern Utah). *Tectonics* **6**, 423–48. doi: 10.1029/tc006i004p00423.

Malavieille J (1987b) Kinematics of compressional and extensional ductile shearing deformation in a metamorphic core complex of the northeastern basin and range. *Journal of Structural Geology* **9**, 541–54. doi: 10.1016/0191-8141(87)90139-8.

Marchesini B, Garofalo PS, Menegon L, Mattila J and Viola G (2019) Fluid-mediated, brittle–ductile deformation at seismogenic depth–Part 1: fluid record and deformation history of fault veins in a nuclear waste repository (Olkiluoto Island, Finland). *Solid Earth* **10**, 809–38.

McCaig AM (1988) Deep fluid circulation in fault zones. *Geology* **16**, 867–70.

Menegon L and Fagereng Å (2021) Tectonic pressure gradients during viscous creep drive fluid flow and brittle failure at the base of the seismogenic zone. *Geology* **49**, 1255–9.

Menegon L, Fusseis F, Stünitz H and Xiao X (2015) Creep cavitation bands control porosity and fluid flow in lower crustal shear zones. *Geology* **43**, 227–30.

Methner K, Mulch A, Teyssier C, Wells ML, Cosca MA, Gottardi R, Gébelin A and Chamberlain CP (2015) Eocene and Miocene extension, meteoric fluid infiltration, and core complex formation in the Great Basin (Raft River Mountains, Utah). *Tectonics* **34**, 680–93.

Miller DM (1980) Structural geology of the northern Albion Mountains, south-central Idaho. In *Cordilleran Metamorphic Core Complexes* (eds MD Crittenden, PJ Coney and GH Davis), pp. 399–423. Geological Society of America Memoir vol. 153.

Miller SA (2013) The role of fluids in tectonic and earthquake processes. In *Advances in Geophysics, vol. 54* (ed. R Dmowska), pp. 1–46. Amsterdam: Elsevier.

Morrison J and Anderson JL (1998) Footwall refrigeration along a detachment fault: implications for the thermal evolution of core complexes. *Science* **279**, 63–6.

Prando F, Menegon L, Anderson M, Marchesini B, Mattila J and Viola G (2020) Fluid-mediated, brittle–ductile deformation at seismogenic depth–Part 2: stress history and fluid pressure variations in a shear zone in a nuclear waste repository (Olkiluoto Island, Finland). *Solid Earth* **11**, 489–511.

Précigout J, Stünitz H and Villeneuve J (2019) Excess water storage induced by viscous strain localization during high-pressure shear experiment. *Scientific Reports* **9**, 3463. doi: 10.1038/s41598-019-40020-y.

Quilichini A, Siebenaller L, Nachlas WO, Teyssier C, Vennemann TW, Heizler MT and Mulch A (2015) Infiltration of meteoric fluids in an extensional detachment shear zone (Kettle dome, WA, USA): how quartz dynamic recrystallization relates to fluid-rock interaction. *Journal of Structural Geology* **71**, 71–85.

Reynolds SJ and Lister GS (1987) Structural aspects of fluid-rock interactions in detachment zones. *Geology* **15**, 362–6.

Roedder E (1984) *Fluid Inclusions*. Reviews in Mineralogy, Volume 12. Washington, DC: Mineralogical Society of America.

Sabisky M (1985) Ductile flow and folding in the Raft River Mountains, northwestern Utah. *Eos* **66**, 1089.

Saltzer SD and Hodges KV (1988) The Middle Mountain shear zone, southern Idaho: kinematic analysis of an early Tertiary high-temperature detachment. *Geological Society of America Bulletin* **100**, 96–103. doi: 10.1130/0016-7606(1988)100<0096:tmmszs>2.3.co;2.

Schneider CA, Rasband WS and Eliceiri KW (2012) NIH Image to ImageJ: 25 years of image analysis. *Nature Methods* **9**, 671–5. doi: 10.1038/nmeth.2089.

Shimizu I (1995) Kinetics of pressure solution creep in quartz: theoretical considerations. *Tectonophysics* **245**, 121–34.

Sibson RH (1974) Frictional constraints on thrust, wrench and normal faults. *Nature* **249**, 542–4.

Sibson RH (1977) Fault rocks and fault mechanisms. *Journal of the Geological Society, London* **133**, 191–213.

Sibson RH (1990) Conditions for fault-valve behaviour. In *Deformation Mechanisms, Rheology and Tectonics* (eds RJ Knipe and EH Rutter), pp. 15–28. Geological Society of London, Special Publication no. 54.

Sibson RH (1992) Fault-valve behavior and the hydrostatic-lithostatic fluid pressure interface. *Earth-Science Reviews* **32**, 141–4.

Sibson RH (2000) Fluid involvement in normal faulting. *Journal of Geodynamics* **29**, 469–99.

Siebenaller L, Boiron MC, Vanderhaeghe O, Hibsch C, Jessell MW, Andre-Mayer AS and Photiades A (2013) Fluid record of rock exhumation across the brittle–ductile transition during formation of a Metamorphic Core Complex (Naxos Island, Cyclades, Greece). *Journal of Metamorphic Geology* **31**, 313–38.

Siebenaller L, Vanderhaeghe O, Jessell M, Boiron MC and Hibsch C (2016) Syntectonic fluids redistribution and circulation coupled to quartz recrystallization in the ductile crust (Naxos Island, Cyclades, Greece). *Journal of Geodynamics* **101**, 129–41.

Stipp M, Stunitz H, Heilbronner R and Schmid SM (2002) The eastern Tonale fault zone: a 'natural laboratory' for crystal plastic deformation of quartz over a temperature range from 250 to 700 C. *Journal of Structural Geology* **24**, 1861–84. doi: 10.1016/s0191-8141(02)00035-4.

Sullivan WA (2008) Significance of transport-parallel strain variations in part of the Raft River shear zone, Raft River Mountains, Utah, USA. *Journal of Structural Geology* **30**, 138–58. doi: 10.1016/j.jsg.2007.11.007.

Todd VR (1980) Structure and petrology of a Tertiary gneiss dome in northwestern Utah. In *Cordilleran Metamorphic Core Complexes* (eds MD Crittenden, PJ Coney and GH Davis), pp. 349–83. Geological Society of America Memoir vol. 153.

Trepmann CA and Seybold L (2019) Deformation at low and high stress-loading rates. *Geoscience Frontiers* **10**, 43–54. doi: 10.1016/j.gsf.2018.05.002.

Trepmann CA and Stöckhert B (2003) Quartz microstructures developed during non-steady state plastic flow at rapidly decaying stress and strain rate. *Journal of Structural Geology* **25**, 2035–51.

Vityk MO and Bodnar RJ (1995) Textural evolution of synthetic fluid inclusions in quartz during reequilibration, with applications to tectonic reconstruction. *Contributions to Mineralogy and Petrology* **121**, 309–23. doi: 10.1007/bf02688246.

Vollmer FW (2015) Orient 3: a new integrated software program for orientation data analysis, kinematic analysis, spherical projections, and Schmidt plots. *Geological Society of America Abstracts with Programs* **47**, 49.

Wehrens P, Berger A, Peters M, Spillmann T and Herwegh M (2016) Deformation at the frictional-viscous transition: evidence for cycles of fluid-assisted embrittlement and ductile deformation in the granitoid crust. *Tectonophysics* **693**, 66–84.

Wells ML (1997) Alternating contraction and extension in the hinterlands of orogenic belts: an example from the Raft River Mountains, Utah. *Geological Society of America Bulletin* **109**, 107–26. doi: 10.1130/0016-7606(1997)109<0107:acaeit>2.3.co;2.

Wells ML (2001) Rheological control on the initial geometry of the Raft River detachment fault and shear zone, western United States. *Tectonics* **20**, 435–57. doi: 10.1029/2000tc001202.

Wells ML, Hoisch TD, Peters MT, Miller DM, Wolff ED and Hanson LM (1998) The Mahogany Peaks Fault, a Late Cretaceous–Paleocene(?) normal fault in the hinterland of the Sevier Orogen. *The Journal of Geology* **106**, 623–34. doi: 10.1086/516046.

Wells ML, Snee LW and Blythe AE (2000) Dating of major normal fault systems using thermochronology: an example from the Raft River detachment, Basin and Range, western United States. *Journal of Geophysical Research: Solid Earth* **105**, 16303–27. doi: 10.1029/2000jb900094.

Whitney DL, Teyssier C, Rey P and Buck WR (2013) Continental and oceanic core complexes. *Geological Society of America Bulletin* **125**, 273–98.

Zhu W, Allison KL, Dunham EM and Yang Y (2020) Fault valving and pore pressure evolution in simulations of earthquake sequences and aseismic slip. *Nature Communications* **11**, 4833. doi: 10.1038/s41467-020-18598-z.